metals

MDPI

Article

Effects of Diatomite Contents on Microstructure, Microhardness, Bioactivity and Biocompatibility of Gradient Bioceramic Coating Prepared by Laser Cladding

Guofen Zhang [1] and Qibin Liu [1,2,*]

[1] College of Materials and Metallurgy, Guizhou University, Guiyang 550025, China; zguofen112@163.com
[2] Key Laboratory of Advanced Manufacturing Technology, Ministry of Education, Guizhou University, Guiyang 550025, China
* Correspondence: qbliugzu@163.com

Abstract: Biometallic materials are widely used in medicine because of excellent mechanical properties. However, biometallic materials are limited in the application of biomaterials due to their lack of bioactivity. To solve this problem, a gradient bioceramic coating doped with diatomite (DE) was successfully fabricated on the surface of Ti6Al4V alloy by using the broadband-laser cladding process to improve the bioactivity of metal materials. As well as the DE contents on the microstructure, microhardness, bioactivity and biocompatibility were investigated. The experimental results demonstrate that the addition of moderate amounts of DE is effective in reducing the number of cracks. The X-ray diffraction (XRD) results reveal that the bioceramic coating doped with DE mainly consists of $CaTiO_3$, hydroxyapatite (HA), tricalcium phosphate (TCP) and silicate, and that the amount of HA and TCP in the coating reached maximum when the bioceramic coating was doped with 10wt% DE. The bioceramic coating doped with 10wt% DE has favorable ability to deposit bone-like apatite. These results indicate that the addition of DE can improve cracking sensibility, bioactivity and biocompatibility of the coating.

Keywords: broadband-laser cladding; diatomite; gradient bioceramic; bioactivity; biocompatibility

Citation: Zhang, G.; Liu, Q. Effects of Diatomite Contents on Microstructure, Microhardness, Bioactivity and Biocompatibility of Gradient Bioceramic Coating Prepared by Laser Cladding. *Metals* **2022**, *12*, 931. https://doi.org/10.3390/met12060931

Academic Editors: Tomasz Czujko and Antonio Riveiro

Received: 31 March 2022
Accepted: 26 May 2022
Published: 28 May 2022

1. Introduction

The variety of bone defects caused by aging and traffic accidents have expanded the need for bone replacement materials [1–6], thus promoting research and development of bone replacement biomaterials [7–10]. Thus far, biomedical alloys are potential candidates for hard tissue repair materials, as metallic biomaterials can withstand long-term, variable and abrupt loading [11,12]. In recent years, there has been a significant increase in the use of Ti6Al4V alloy, which has the advantages of high strength, high rigidity, low density and corrosion resistance [11–13]. For biological implants, after the biomedical Ti6Al4V alloy is implanted, it cannot form a chemical connection with the biological living tissue, which can easily fall off after a long implantation time because of the lack of bioactivity, and periodic replacement of implant materials can easily cause pain to the patient, thus the medical application of Ti6Al4V alloy is limited. In order to improve the bioactivity and biocompatibility of Ti6Al4V alloy, it is necessary to modify the Ti6Al4V alloy. Hydroxyapatite (HA) and tricalcium phosphate (TCP) with excellent bioactivity are frequently used in biomaterials [14–22].

Calcium-phosphorus bioceramic coatings can enhance the bioactivity and osteogenic properties of biomaterials, and there are various preparation methods for calcium phosphorus bioceramic coatings [23–26]. Hydroxyapatite coatings were deposited by plasma spray technology for orthopedic and dental applications [23]. Apatite coatings were prepared by electrochemical deposition technology under different acidic conditions, which inhibited the activity of osteoclasts, promoted new bone formation and enhanced bone-implant

integration [24]. Eggshell-derived hydroxyapatite coatings were successfully produced and were prepared on titanium alloy surfaces by micro-arc oxidation process [25]. Porous bioceramic coatings were prepared by laser cladding technology to improve the osteogenic properties of the coatings [26]. Bioceramic coatings prepared by laser cladding can obtain bioactive coating materials with high bonding strength and good bioactivity, which can promote bone tissue integration and facilitate bone repair [20,21]. In our previous work, the bioceramic coating with HA and TCP was successfully prepared on Ti6Al4V alloy [17–22], which showed good bioactivity and biocompatibility. Zhang et al. prepared a gradient bioceramic coating doped with La_2O_3 on Ti6Al4V, the result showed that when the content of La_2O_3 is 0.6wt%, the amount of HA + TCP reaches maximum and the proliferation and adhesion of bone cells performed well [22].

In 1969, Larry Hench discovered 45S5 bioglass, which has excellent biocompatibility and bioactivity. The amount of silica in 45S5 bioglass is as high as 46.1mol% [27,28]. Kang et al. reported that homogeneous PEI-silica hybrid material was coated on Mg substrates, which led to no cracks in the coatings [29]. Soluble silica and calcium ions stimulate osteoblasts to produce bone matrix [30]. Diatomite (DE) (90.62wt% SiO_2, 3.53wt% Fe_2O_3, 2.52wt% Na_2O, 1.64wt% Al_2O_3, K_2O, MgO, CaO, P_2O_5, AR), a kind of biogenic siliceous sedimentary rock, which is mainly composed of the remains of ancient diatoms, mainly consists of SiO_2 [31]. Additionally, DE is of lower cost as well as being an abundant resource. In our past work [20], the bioceramic coating doped with DE and SiO_2, respectively, on Ti6Al4V was fabricated by broadband-laser cladding. The results of the study have shown that the DE-doped bioceramic coating has better bioactivity and biocompatibility than the SiO_2-doped bioceramic coating, and the DE-doped bioceramic coating exhibits favorable ability to deposit bone-like apatite, thus the DE-doped bioceramic coating is more suitable as a candidate for biomaterials than the SiO_2-doped bioceramic coating. At present, DE is rarely used in the field of biomedicine, and it is of profound significance to explore the impact of DE on Ca-P bioceramic coating.

In the present paper, gradient Ca-P bioceramic coating doped with DE is fabricated on Ti6Al4V by broadband-laser cladding. Laser cladding technology as a surface modification technology, has been extensively used in the processing and repair of material surfaces. Laser cladding technology can use high heat and high energy to quickly melt the material, and after the laser is removed, the material is rapidly cooled. This feature enables the substrate and the coating to form a metallurgical bond, as well as the substrate and the coating having high bond strength. The advantage of this preparation method is that the process is flexible and the material deformation is small. The bioceramic coating is prepared by metallurgical combination of biomedical metal and ceramic powder with favorable biological properties by laser cladding technology. The microstructure of the coating is observed by metallographic microscope. The samples are co-cultured with MG63 human osteosarcoma cells, and the number and morphology of the cells are characterized. The samples are immersed in simulated body fluids (SBF) to characterize the quantity and morphology of bone-like apatite deposited on the coating surface. The effect of DE contents on the microstructure, microhardness, biocompatibility and bioactivity of the coating is systematically investigated.

2. Materials and Methods

2.1. Coating Preparation

The Ti6Al4V was manufactured by the Northwest Institute for Non-ferrous Metal Research, which is used as the substrate. The Ti6Al4V was polished with sandpaper to remove the oxide layer on the substrate. Ti (45–50 μm, AR), $CaCO_3$, $CaHPO_4 \cdot 2H_2O$, La_2O_3 and DE powder (1–5 μm, AR) were weighed. All powders were bought from Kermel Chemical Reagents (Kermel, Tianjin, China). The components of DE were designed to be 5wt% DE, 10wt% DE and 15wt% DE, respectively. The compositional design of the gradient coating is shown in Table 1. The *X* in the table represents the mass fraction of DE, and a control group without doped DE was designed. Putting the powders and absolute ethanol

into the grinding tank, absolute ethanol needs to submerge the powder, and the grinding time is eight hours. The grinded powder was put into a drying oven at 65 °C. The RC-LMS-6000-R laser machine system (Raycus, Wuhan, China) is equipped with an optical fiber with a length of 20 m and a core diameter of 100 μm, which is connected to the laser processing head. The output connector is high quartz block head (HQBH), and the beam quality is less than 4.5 mm·mrad, and the laser machine is in continuous/modulated mode. The laser machine is a continuously tunable fiber laser machine. The laser system is equipped with an RC52 laser cladding head (Raycham, Nanjing, China). After the optical fiber is transmitted through the laser, it is collimated and focused to realize the laser cladding function. The maximum output power of the laser is 6 kW, the polarization direction is random, the wavelength is 1080 nm, the emission angle is less than or equal to 0.1 rad and the modulation frequency range is 50–5 k (Hz). Based on the following laser process parameters of the RC-LMS-6000-R laser machine, output of power P = 5 kW, scanning velocity V = 7 mm·s^{-1}, the focal length is 300 mm, the laser beam size is 2 × 20 (mm^2) and the shielding gas is argon. The dried powder mixed with adhesive (epoxy resin) of the first layer was uniformly placed on the surface of the Ti6Al4V; the thickness of the preset powder was 0.5 mm. After the coating was completely dry, the first gradient layer powders were coated on Ti6Al4V by broadband laser cladding according to the above parameters. Broadband laser cladding can make the molten pool exist for a longer time, the solidification speed is slower and the substances in the molten pool can react more fully, thus broadband laser cladding can obtain a better quality cladding coating. In broadband laser cladding, broadband means that the spot size is a rectangular spot. The second gradient layer was then clad after cleaning, followed by the third gradient layer cladding under the same methods and parameters. A diagrammatic sketch of the laser cladding is shown in Figure 1. Laser cladding technology [17–21,26] is used to irradiate powder materials with high-energy laser beams to melt the powder materials on the surface of the substrate, thereby obtaining a coating with excellent properties. The high-temperature heating of laser cladding can melt the powder material on the surface of the substrate, and a molten pool will be formed on the surface of the substrate, and the powder material will undergo chemical reactions in the molten pool. Therefore, the coating prepared by laser cladding has the characteristics of high bonding strength. In our previous work [32], we tested the bonding strength of gradient bioceramic coatings. A test rod is vertically bonded to the surface of the bioceramic coating with the adhesive. The three experimental fractures occurred between the bioceramic coating and the binder, but not between the bioceramic coating and the titanium alloy, which indicates that the bonding strength between the bioceramic layer and the titanium alloy is greater than the bonding strength between the bioceramic layer and the binder. The results of the three experiments were 35.5 MPa, 37.8 MPa and 38.6 MPa. The average bond strength of the three experiments was 37.3 MPa. The experimental results show that the bonding strength between the broadband laser cladding bioceramic coating and the titanium alloy substrate is above 37.3 MPa. The chemical reaction equations that may occur during the laser cladding process are as follows [20]:

$$CaHPO_4 \cdot 2H_2O \xrightarrow{161–196\ ^\circ C} CaHPO_4 + H_2O \quad (1)$$

$$2CaHPO_4 \xrightarrow{434\ ^\circ C} \gamma\text{-}Ca_2P_2O_7 + H_2O\uparrow \quad (2)$$

$$\gamma\text{-}Ca_2P_2O_7 \xrightarrow{784\ ^\circ C} \beta\text{-}Ca_2P_2O_7 \quad (3)$$

$$CaCO_3 \xrightarrow{825–896\ ^\circ C} CaO + CO_2\uparrow \quad (4)$$

$$\beta\text{-}Ca_2P_2O_7 + CaO \xrightarrow{784\ ^\circ C} Ca_3(PO_4)_2 \quad (5)$$

$$3Ca_3(PO_4)_2 + CaO + H_2O\uparrow \xrightarrow{\Delta} Ca_{10}(PO_4)_6(OH)_2 \quad (6)$$

$$CaO + TiO_2 \xrightarrow{1350\ ^\circ C} CaTiO_3 \quad (7)$$

$$2CaO + SiO_2 \xrightarrow{\Delta} Ca_2SiO_4 \quad (8)$$

$$Ca_3(PO_4)_2 + 2CaO + SiO_2 \xrightarrow{\Delta} Ca_5(PO_4)_2SiO_4 \quad (9)$$

Table 1. Compositional design of gradient coating.

Coating Layers	81.12wt% $CaHPO_4 \cdot 2H_2O$ + 18.88wt% $CaCO_3$ + 0.6wt% La_2O_3 + *X*wt% DE	Ti Powders
Coating layer 1/g	30	70
Coating layer 2/g	70	30
Coating layer 3/g	100	0

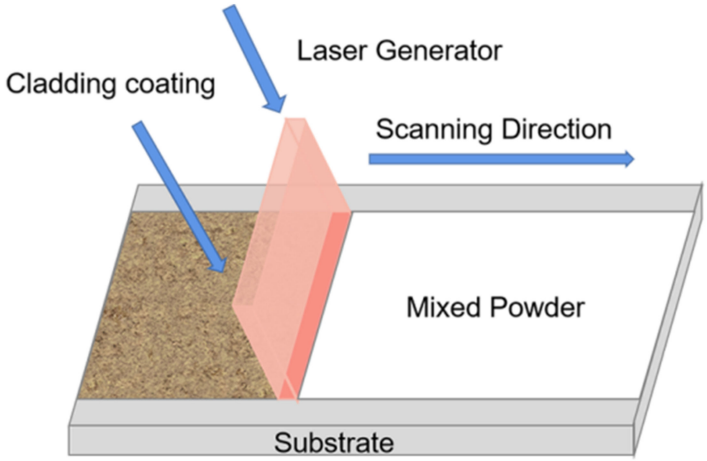

Figure 1. Diagrammatic sketch of broadband-laser cladding.

2.2. Evaluation of X-ray diffraction (XRD)

Phase analysis of the coating was characterized using the BrukerAXS D8 Advance Krystalloflex X-ray diffractometer (Bruker, Karlsruhe, Germany) using Cu Karadiation at 40 kV and 40 mA from 10 to 80° with a step size of 0.02° at room temperature. The experiment was repeated three times.

2.3. Evaluation of Cross-Section

The cladding sample was metallographically polished with SiC grit paper, and the samples were then polished with alumina polishing agent, and then the cross section of the sample was clean. The microstructure of the cross-section was observed with an inverted metallurgical microscope—OMOLYMPUS GX51(Olympus Corporation, Tokyo, Japan). The microhardness of the coating was measured by microhardness tester (DHV-1000Z, Shuangxu Electronics Co., Ltd., Shanghai, China) from ceramic layer to the substrate at a distance of 0.1 mm. The test force is 1 kg and the holding time is 15 s. The experiment was repeated three times.

2.4. Evaluation of Vitro Cell Compatibility

The human osteosarcoma cell line MG63 was used for the cytotoxicity tests. Prior to the cytotoxicity tests, the samples were autoclaved by 120 °C autoclave; subsequently the samples were exposed to UV light for over three hours on the bench. The cells in the culture flask were incubated in the incubator for full growth, and the cells were inoculated onto the coating. Cells and the samples were co-cultivated on a 24-well plate. MG63 cells (10^4 cells·mL^{-1}, 1 mL) were cultured on samples at 37 °C in a 5% CO_2 atmosphere for 1 day. Furthermore, 100 µL Counting Kit-8 (cck-8) was added to well tissue culture test plates and incubated for 3 h. The cck8 kit contains metho electron coupling reagent, which can be reduced to orange-yellow water-soluble formazan. The more cells proliferate and

the faster, the darker the color, and the more cytotoxic, the lighter the color. Finally, the absorbance at 450 nm of the solution in each well was measured by an enzyme-linked analyzer (THERMO Varioskan Flash, TherERMO Varioskan Flash, Therfisher, Waltham Mass, MA, USA). The same method was used to obtain absorbance on the third day and the fifth day. The experiment was repeated three times.

After the samples had been autoclaved and sterilized by ultraviolet light, the samples and cells were co-cultured. The fluorescein diacetate (FDA) master batch of 5 $mg \cdot mL^{-1}$ prepared with acetone was stored at −4 °C, 20 $\mu l \cdot mL^{-1}$ solution of FDA master mix and phosphate buffered solution (PBS) was placed into a 96-well plate and incubated in an incubator for 8 min, after which the cell morphology was observed by confocal laser scanning microscope (TCS SP8, Leica, Hesse-Darmstadt, Germany). The various biological reagents and all cells used in this study were purchased from Kermel Chemical Reagents (Kermel, Tianjin, China). The experiment was repeated three times. Biocompatibility was tested by in vitro cytotoxicity test and fluorescent staining test. Using MG63 cells to co-culture with the coating, the number of cells increased with time, and the cell morphology did not change abnormally, indicating that the material has good biocompatibility.

2.5. Cell Morphology

Samples were cultured for 3 days, washed twice with PBS, and fixed with 3% glutaraldehyde at 4 °C for 24 h. The samples were washed twice with PBS, and subsequently dehydrated in an ethanol series for 15 min (30%, 50%, 70%, 95% and 100%, three times). The samples were dried in a vacuum drying oven, after which samples were sprayed with gold; cell morphology was observed by scanning electron microscopy (SEM, ZEISS Gemini 300, Berlin, Germany). The experiment was repeated three times.

2.6. Evaluation of In Vitro Bioactivity

Bioactive materials are realized by the deposition of HA at the interface and can be associated with living tissues. Therefore, under normal circumstances, the amount of HA produced by the sample is used to evaluate the bioactivity of the sample. SBF were prepared according to a study by Kokubo and Takadama [33]. The 5 mL SBF solution and sample were placed together in thermostatic shakers (ZWY-1102C, ZHCHENG, Shanghai, China) at 37 °C; SBF solution was replaced after 48 h. Samples soaked for 7 and 14 days were removed and washed with deionized water and the samples were dried in a vacuum drying oven. The surficial morphology of the coating was observed by scanning electron microscopy (SEM, ZEISS Gemini 300, Berlin, Germany). Phase analysis of the coating was characterized by the BrukerAXS D8 Advance Krystalloflex X-ray diffractometer. The experiment was repeated three times.

2.7. Statistical Analysis

All data were expressed as the mean ± standard deviation. p-values less than 0.05 were considered statistically significant in all cases.

3. Results

The Ca-P coatings doped with DE consist mainly of HA, TCP, CPS ($Ca_5(PO_4)SiO_4$) and Ca_2SiO_4, and $CaTiO_3$ phases, as can be seen from Figure 2. After the addition of DE, the crystallinity of $CaTiO_3$ phases (around 59° and 70°) are significantly weaker; the crystallinity of HA, TCP and CPS phases are increased obviously, especially in the vicinity of 30° and 40°, the TCP characteristic peaks of the 10wt% DE coating are obvious. The new phases can be seen from the Ca-P coatings doped with 5wt% DE, 10wt% DE and 15wt% DE compared with non-doped, such as CPS and Ca_2SiO_4, the new diffraction peak corresponding to TCP appears around 30° of diffraction angle 2θ. With the increase of DE, the intensity of the characteristic diffraction peaks of HA + TCP phase gradually increase and then decrease. The Ca-P coating doped with 10wt% DE produces the most HA, TCP

and silicate phases. When the bioceramic coating is doped with 15wt% DE, more calcium silicate (around 24°) and CPS (around 48°) are produced.

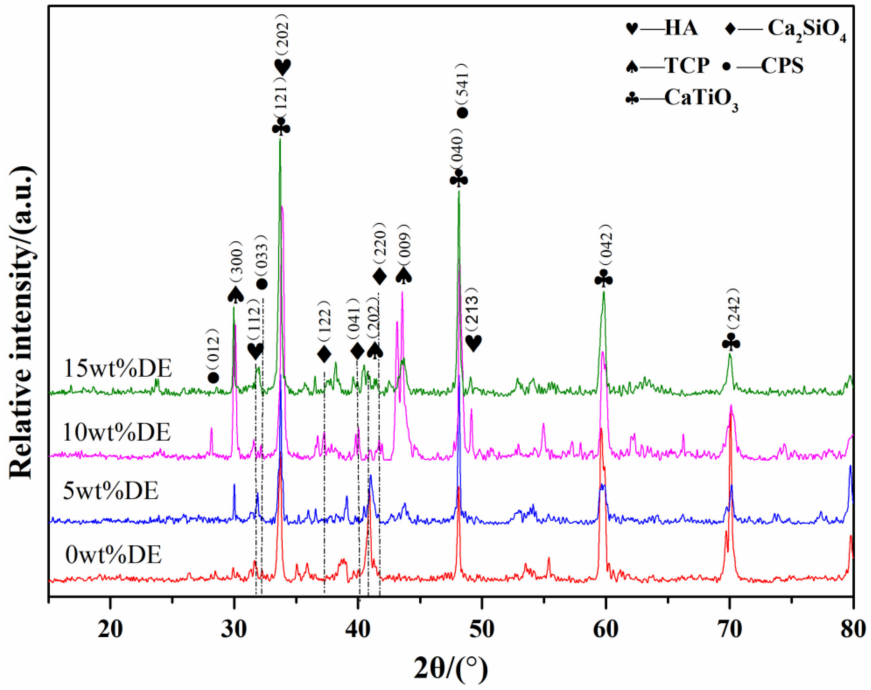

Figure 2. XRD patterns of bioceramic coating with different contents of DE (0wt%, 5wt%, 10wt% and 15wt%).

3.1. Microstructure Analysis

The cross-sectional microstructure of coatings is shown in Figure 3. It is seen that the bioceramic coatings doped with DE consist of three layers, which are the substrate, the alloy layer and ceramic layer from bottom to top. The gradient coating that we designed was successfully developed by broadband-laser cladding. It is also seen from Figure 3 that the cracks of the coatings are extended from the ceramic coating to the alloy layer. As the DE-doped content increases, the cracks of the cross section gradually decrease and then increase. As can be seen from Figure 3, the most cracks are found on the Ca-P coatings doped with 0wt% DE and 15wt% DE, and the width of the cracks are the largest, which contains not only longitudinal cracks but also transverse cracks. No transverse cracks and very few longitudinal cracks are evident in the Ca-P coatings doped with 5wt% DE and 10wt% DE.

Microhardness analysis of La_2O_3-doped gradient coatings with different contents of DE (0wt%, 5wt%, 10wt% and 15wt%) are shown in Figure 4. As can be seen from Figure 4, the microhardness of the ceramic layer and the alloy layer are higher than that of the substrate. From the ceramic layer to the alloy layer and then to the substrate, the microhardness gradually increases and then decreases. It can be seen from Figure 4 that the average hardness of the bioceramic coating doped with 5wt% DE is the highest.

3.2. Analysis of In Vitro Cell Compatibility

Optical density (OD) assay of MG63 cell on coatings doped with DE (0wt%, 5wt%, 10wt%, and 15wt%) at 1 d, 3 d and 5 d is showed in Figure 5. It can be seen that the OD value of MG63 cell gradually increases as time increases. There is no noticeable difference in the amount of MG63 cell co-cultured with each coating at 1 d. The OD value of Ca-P coatings doped with different DE contents are significantly different at 3 d, the OD value of the Ca-P coatings doped with 10wt% DE reach the maximum at 3 d. The situation at 5 d is similar to that at 3 d. As the content of DE increases, the OD value gradually increases and then decreases.

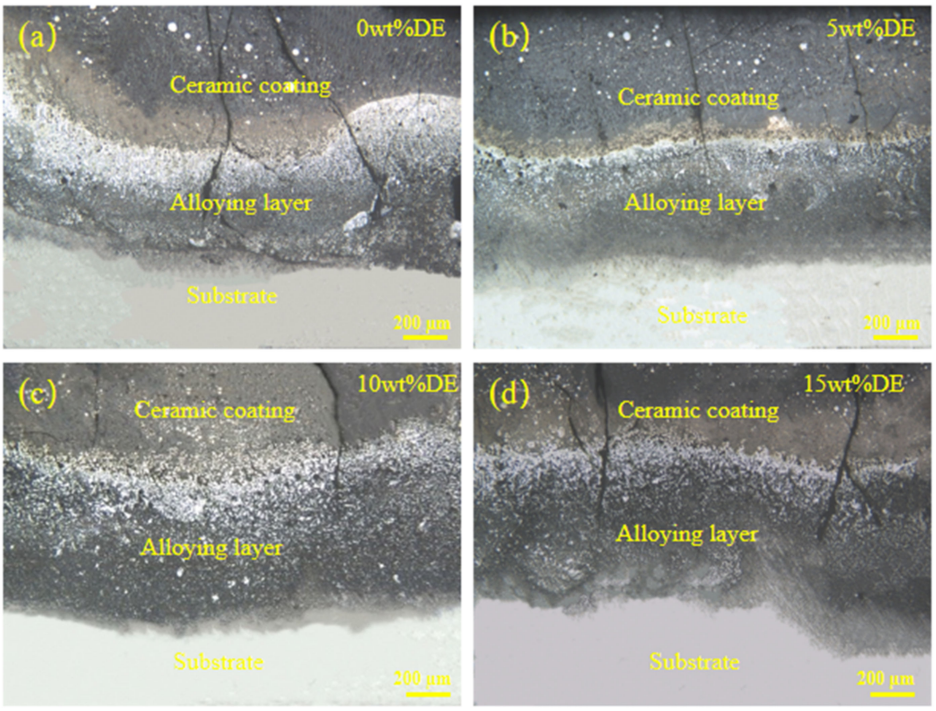

Figure 3. Cross-sectional microstructure of bioceramic coating with different contents of DE, (**a**) 0wt%; (**b**) 5wt%; (**c**) 10wt%; (**d**) 15wt%.

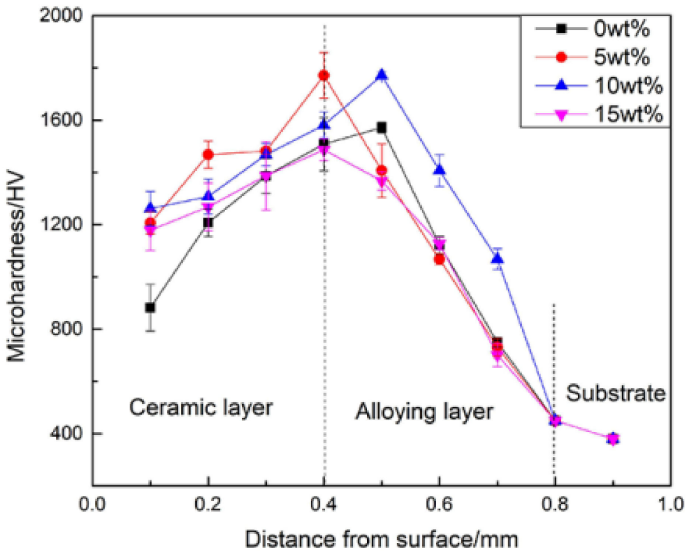

Figure 4. Microhardness analysis of bioceramic coating with different contents of DE (0wt%, 5wt%, 10wt% and 15wt%).

Fluorescent images of MG63 cell co-cultured with coatings at 3 d are shown in Figure 6. As can be seen from Figure 6, cell morphology is maintained well, indicating that the Ca-P bioceramic coating doped with DE has favorable compatibility with the cell. As the content of DE gradually increases, the number of cells contained in the coating gradually increases and then decreases. The coatings doped with 10wt% DE and 15wt% DE contain a large number of cells, and MG63 cells have good cell morphology with spindle-shaped growth.

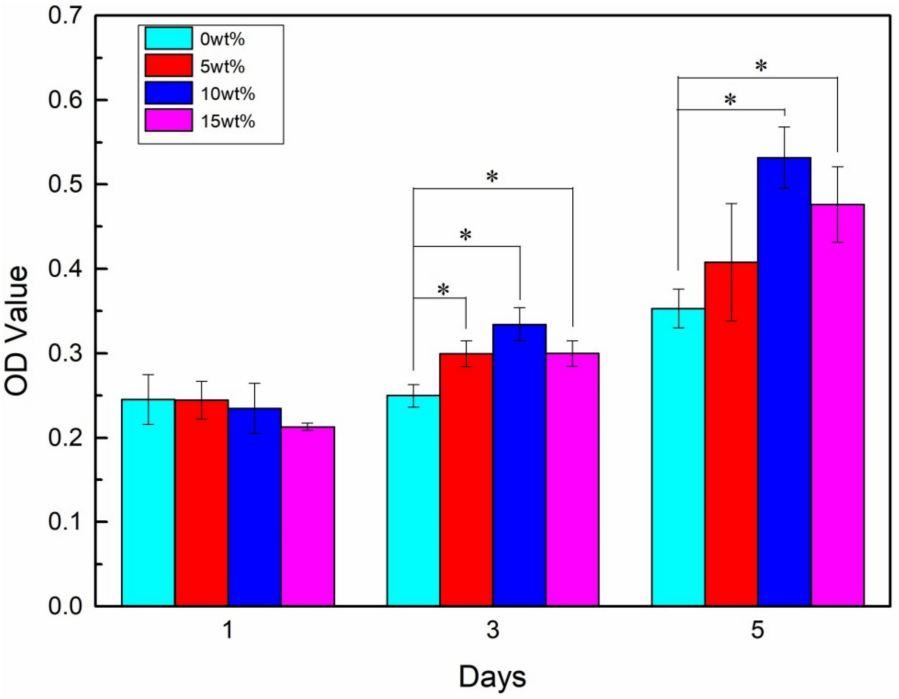

Figure 5. Optical density (OD) assay of MG63 cell on coatings with DE (0wt%, 5wt%, 10wt% and 15wt%) at 1 d, 3 d and 5 d. (* $p < 0.05$).

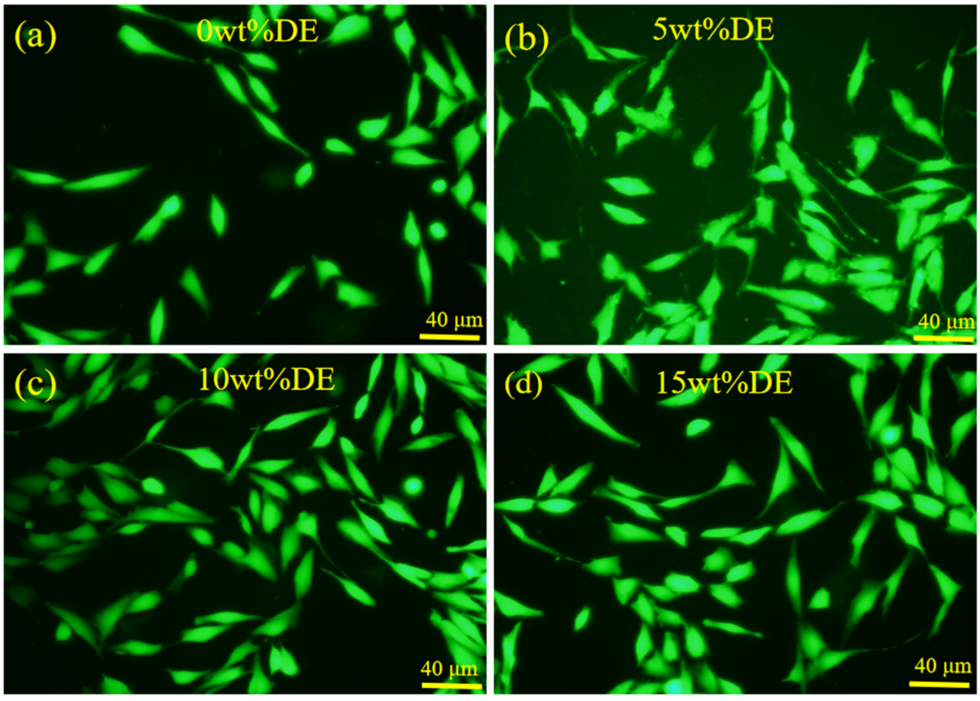

Figure 6. Fluorescent images of MG63 cell on coatings with different contents of DE at 3 d, (**a**) 0wt%; (**b**) 5wt%; (**c**) 10wt%; (**d**) 15wt%.

3.3. Cell Morphology

SEM images depict MG63 morphology after 3 d co-culture with coatings doped with 0wt% DE, 5wt% DE, 10wt% DE and 15wt% DE are shown in Figure 7. It is seen from Figure 7 that the Ca-P coatings non-doped with DE and the Ca-P coatings doped with DE have cells adhered to the layer, and many pseudopodia are observed in the cells on bioceramic coatings, indicating that the cell extending is favorable. The MG63 cells on the coating

doped with 10wt% DE coating are connected to one piece, the pseudopodium also grips the coating tightly, it shows that the bioceramic coatings have favorable biocompatibility and osteogenic properties on osteoblast MG63 cells.

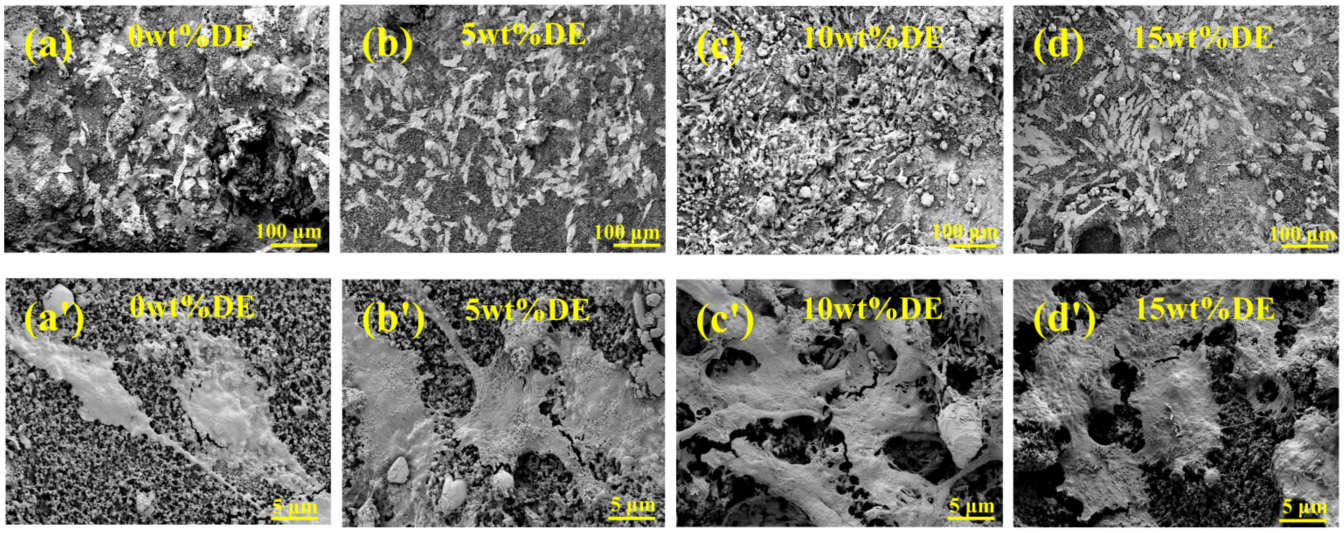

Figure 7. Cell growth morphology of MG63 cells at 3 d on coatings with different contents of DE, (**a**,**a′**) 0wt% DE; (**b**,**b′**) 5wt% DE; (**c**,**c′**) 10wt% DE; (**d**,**d′**) 15wt% DE.

3.4. Analysis of In Vitro Bioactivity

SEM images of the coatings with different DE contents before and after immersion for 7 d and 14 d in SBF are shown in Figure 8. The sediments are formed on the surface of the bioceramic coatings doped with 5wt% DE, 10wt% DE and 15wt% DE compared with the non-doped coating after immersion in SBF for 7 d and 14 d. As can be seen from Figure 8, the Ca-P coating doped with 10wt% DE produces the most sediments. The shape of the sediment is mainly the hippocampus shape close to the surface and the three-dimensional chrysanthemum bud shape. From the energy spectrum analysis, it can be observed that the Ca/P of the hippocampus shape substance at point A is 1.74, and the Ca/P of the chrysanthemum bud shape substance at point B is 1.69. The Ca/P of the two substances is close to the theoretical Ca/P (1.67) of HA [12], the sediment is bone-like apatite. From the element mapping diagram of calcium phosphate silicon, it can be observed that the element distribution of CPS is uniform with the addition of DE.

XRD patterns of Ca-P coatings doped with different DE contents for separate soaking times are shown in Figure 9. The Ca-P coatings doped with DE consist mainly of HA, TCP, CPS, CaO and Ca_2SiO_4 and $CaTiO_3$ phases. It can be seen that the characteristic diffraction peaks of HA on the coating are enhanced after 7 d (14 d) of immersion for each coating. Diffraction peak intensity of HA in DE-doped coatings is significantly higher than that in the non-doped coating. During the soaking of the coating in SBF, the HA originally present in the coating can promote the formation of bone-like apatite. Bioceramic coatings with different DE contents have obvious characteristic diffraction peaks of CaO at around 37° after soaking in SBF. The reason for the appearance of CaO may be that the coating is soaked in SBF, and the TCP degradation reaction generates CaO.

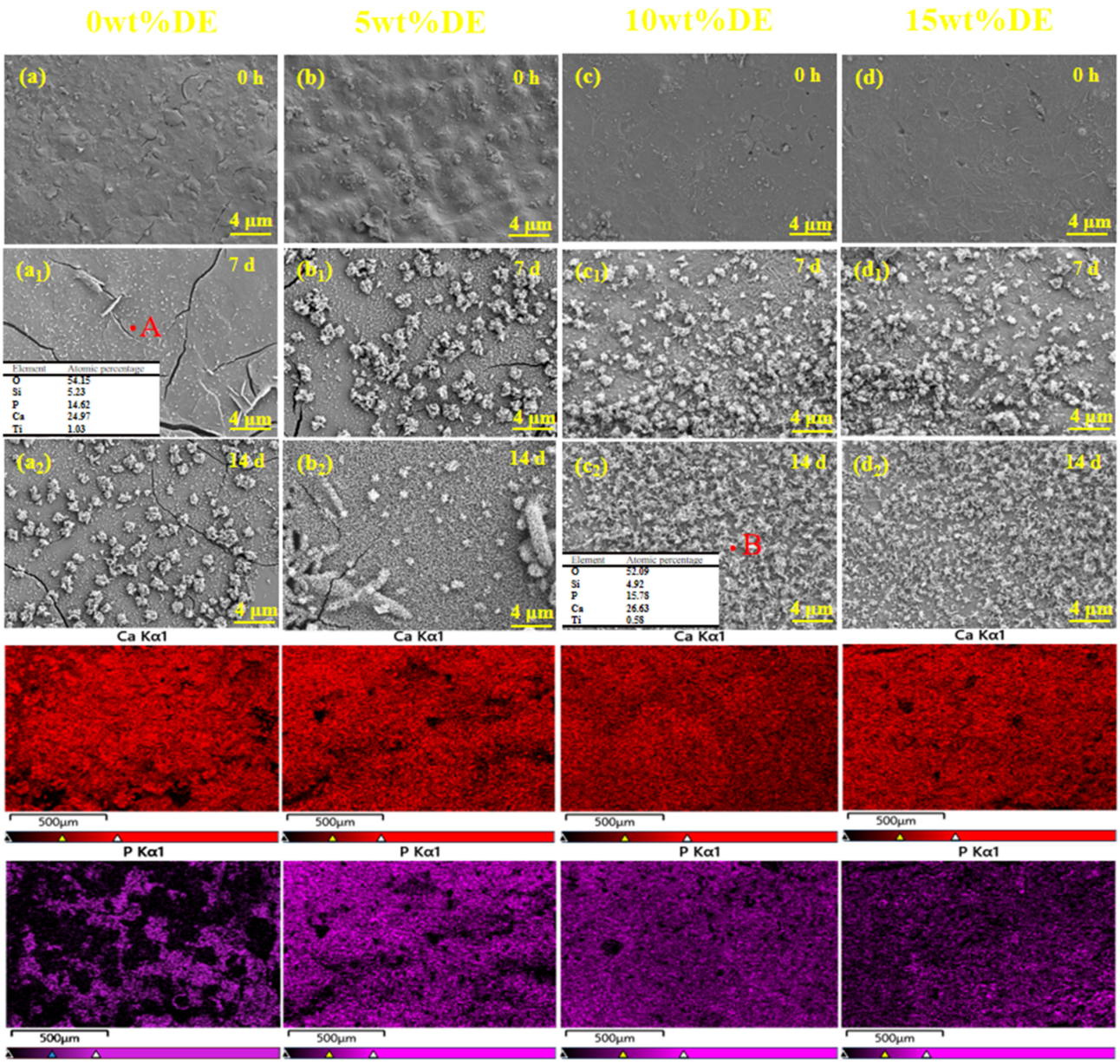

Figure 8. The biomineralization of Ca-P coatings after being soaked in SBF for 7 d and 14 d including: surface morphologies of coatings without soaking (**a**–**d**), and coatings after soaking in SBF for 7 d (**a**$_1$–**d**$_1$) and 14 d (**a**$_2$–**d**$_2$); EDS point scan of points A and B, and elemental mapping images of calcium and phosphate after soaking in SBF for 14 d.

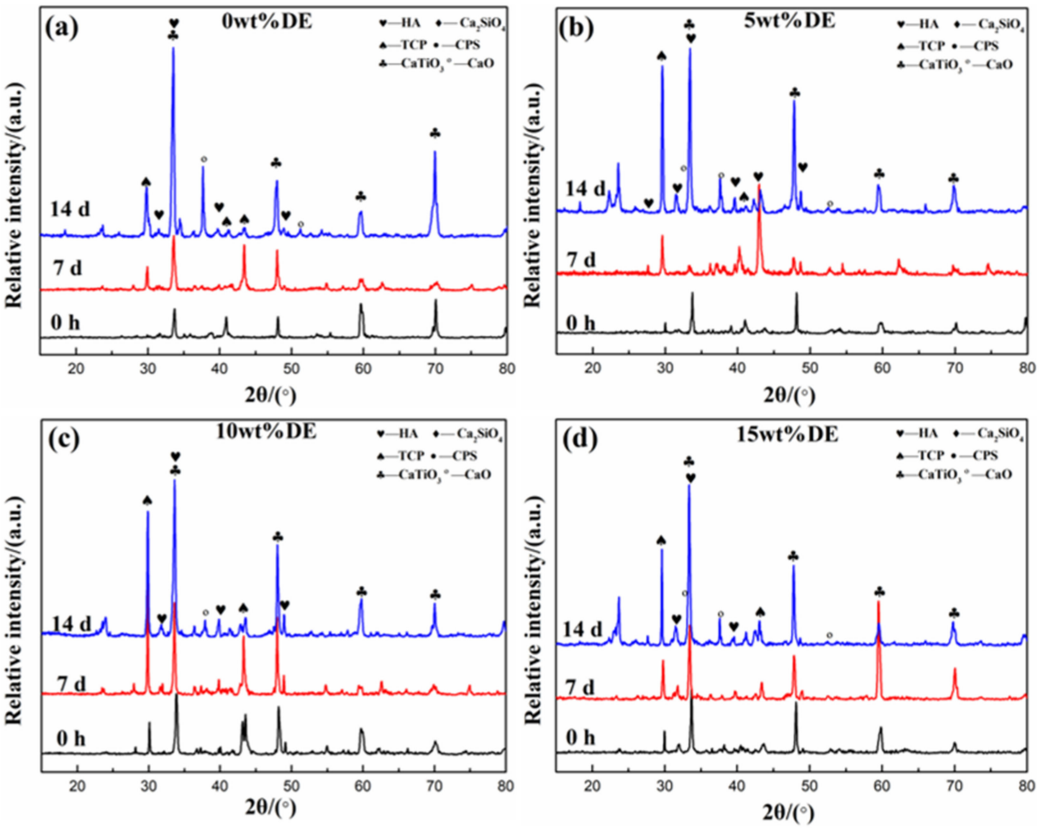

Figure 9. XRD patterns of bioceramic coatings with different contents of DE, (**a**) 0wt% DE; (**b**) 5wt% DE; (**c**) 10wt% DE; (**d**) 15wt% DE, before (0 h) and after (7 d, 14 d) soaking in SBF.

4. Discussion

The significance of this study is to improve the osteogenic and mechanical properties of bone implants through fabricating Ca-P gradient bioceramic coatings doped with DE by broadband-laser cladding. Ca-P coatings doped with natural, harmless and porous DE are fabricated on Ti6Al4V by broadband-laser cladding, which is a low cost and high efficiency method, which further improves the cracking sensibility and biological properties of Ca-P gradient bioceramic coatings. The results demonstrate that the gradient bioceramic coating doped with DE is successfully prepared by broadband-laser cladding. The bonding strength of the bioceramic coating is a factor worth considering for bone implants. Owing to the rapid heating and cooling characteristics of laser cladding, cracks are inevitably formed in the coating [26]. As can be seen from Figure 3 where the addition of DE can dramatically reduce cracks. It is well known that the bond between the oxygen element and silicon element in silicate is an ionic bond and a covalent bond—both the ionic bond and the covalent bond have high strength, thus silicate usually has high strength. Based on the analysis of X-ray diffraction intensity, a large number of HA, TCP, CPS and calcium silicate are produced in the Ca-P coating doped with 10wt% DE. Based on the work of Yoo et al., it is possible to explain why the addition of a moderate amount of DE contributes toward the generation of bioactive phases and they reported [34] that the addition of silica accelerated the transfer of the material and led to a rapid microstructural evolution. The concave angle created by twin boundaries provides more growth sites and increases the growth rate of the crystals, therefore meaning that the appropriate addition of elemental silica increases the nucleation rate of the material. Therefore, it can be assumed that the addition of the appropriate amount of silicon elemental contributes toward the microstructural evolution of the melt pool and facilitates the catalytic synthesis of the bioactive phase with more nucleation sites provided by the silicon elemental. Due to the loose and porous structure of DE, as well as the porosity and enhanced surface area of DE, it allows the added material to

mix with DE uniformly and increases the chance of reaction; and more bioactive phases are generated. As can be seen from Figure 2, the coating doped with 15wt% DE does not work very well, probably due to the excessive amount of DE and other reactants generating many non-bioactive phases. The coating doped with 10wt% DE has extraordinary strength and the coating doped with 10wt% DE has only a small number of cracks. After implantation, this low number of cracks contributes to the growth of new bone.

It can be seen from Figures 6 and 7 that there are a large number of MG63 cells on the coatings doped with 10wt% DE and 15wt% DE, and the morphology of MG63 cells remains spindle shaped. HA and TCP exhibit excellent biocompatibility and good bioactivity [12]. Moreover, silicon, calcium and phosphorus play significant roles in stimulating osteogenesis and bone metabolism [35]. Silicon can resist oxidation and inflammation, more importantly, silicon can promote the activity of the obtained cell by increasing the expression of type I collagen [36,37]. Calcium silicate-based biomaterials exhibit excellent solubility and osteogenic properties [37] and also contribute toward the proliferation, osteogenic differentiation and bone formation of bone marrow mesenchymal stem cells [38,39]. Si^{4+} has been proven to stimulate proliferation, osteogenic differentiation of osteoblast-like cells [40], suppress osteoclastic differentiation and osteoclast-mediated bone resorption activity [41].

It is clear from work by Zhou et al. [42] that the effect of silicate bioceramics must not be underestimated, as it was reported that silicate bioceramics exhibit better osteogenic potential than β-TCP implants. It can be seen from Figure 2 that the coating doped with 10wt% DE has HA, TCP, CPS and calcium silicate of high diffraction peak intensity. The surface after laser cladding has a certain roughness, and appropriate surface roughness has a certain promoting effect on cell adhesion. Therefore, the Ca-P coating doped with 10wt% DE has many cells, the cell morphology and cell adhesion on the coating are good. This phenomenon indicates that the Ca-P coating doped with 10wt% DE has the ability to support the attachment of osteoblasts, implying that coatings doped with 10wt% DE have good osteoconduction. Stimulation of bone regeneration is considered to be key to the treatment of osteoporotic bone defects [24].

Kokubo et al. [43] reported that due to the presence of silanol-based functional groups, hydroxyapatite-like can be deposited on the bioreplacement materials after soaking SBF. The presence of silanol-based functional groups can be used as an effective site for apatite nucleation on the surface of biomaterials. In physiological solutions, the silicon in biomaterials can form silanol groups on the surface of biomaterials via ion exchange between the material and the surrounding solution [44]. Calcium silicate and CPS produced on the surface of the coating provide the silicon element, thus depositing HA. It can be seen from Figure 2 that a large amount of silicate is produced in the Ca-P coating doped with 10wt% DE, which provides a large number of nucleation sites for the deposition of HA. HA and TCP brought by broadband-laser cladding in the coating can spontaneously grow by consuming calcium and phosphate ions in the surroundings of the physiological solution [45]. Studies have demonstrated that the β-TCP bioceramics incorporated with calcium silicate noticeably improved proliferation and osteogenic differentiation of osteoblast-like cells, as well as markedly stimulated in vivo bone formation and materials degradation [44,46]. Perhaps we should change our habitual thinking that the higher HA + TCP can make the performance of the biomaterial better. For the Ca-P coating, the fact may be that appropriate HA + TCP combined with appropriate silicate can exhibit excellent mechanical and biological properties. The disadvantage of HA and TCP is impoverished mechanical strength [47,48], and the disadvantages of $CaTiO_3$ are inferior biological properties [21]; silicate cannot provide long-term mechanical support for the growth of new bone [44]. Nevertheless, the above substances can be processed by broadband-laser cladding to prepare a desirable bone replacement material with good biological properties and good mechanical properties.

5. Conclusions

In this work, a bioceramic material exhibiting metallurgical bonding between the coating and the substrate was fabricated by broadband-laser cladding method. The bioceramic coating was subjected to phase analysis, biocompatibility and bioactivity measurements, with the results showing that the addition of DE effectively reduces the number of cracks and increases the microhardness of the material. The microstructures of the bioceramic coatings doped with different DE content were found to comprise HA, TCP, CPS and Ca_2SiO_4. Bone-like apatite was found to be formed on the surface of all of the Ca-P coatings, indicating they exhibit good bioactivity. Upon a gradual increase in the DE content of the material, there was a gradual increase in the number of cells present on the coatings, the Ca-P bioceramic coatings doped with 10wt% DE featuring the highest number of cells, indicating that this coating exhibits the best biocompatibility. The porous structure of DE and its high specific surface area provide a large number of potential nucleation sites for reactions to occur with other substances, giving rise to the formation of silicate, TCP and HA, which greatly improve the bioactivity and biocompatibility of the DE-doped Ca-P bioceramic. These properties make the material an excellent candidate for use in orthopedic applications.

Author Contributions: Conceptualization, methodology, investigation, resources, Q.L.; software, validation, formal analysis, data curation, writing—original draft preparation, writing—review and editing, G.Z. All authors have read and agreed to the published version of the manuscript.

Funding: This research was funded by the High-Level Innovative Talents Plan of Guizhou Province, grant number 2015-4009.

Institutional Review Board Statement: Not applicable.

Informed Consent Statement: Not applicable.

Data Availability Statement: The data that support the findings of this study are available from the corresponding author upon reasonable request.

Conflicts of Interest: The authors declare no conflict of interest.

References

1. Shannon, R.O. Effective ionic radii in oxides and fluorides. *Acta Crystallogr. B* **2018**, *25*, 925–946. [CrossRef]
2. Cho, E.H.; Shammas, R.L.; Carney, M.J.; Weissler, J.M.; Bauder, A.R.; Glener, A.D.; Kovach, S.J.; Hollenbeck, S.T.; Levin, L.S. Muscle versus Fasciocutaneous Free Flaps in Lower Extremity Traumatic Reconstruction: A Multicenter Outcomes Analysis. *Plast. Reconstr. Surg.* **2018**, *141*, 191–199. [CrossRef] [PubMed]
3. Lu, Y.; Li, L.H.; Zhu, Y.; Wang, X.L.; Li, M.; Lin, Z.F.; Hu, X.M.; Zhang, Y.; Yin, Q.S.; Xia, H.; et al. Multifunctional Copper-Containing Carboxymethyl Chitosan/Alginate Scaffolds for Eradicating Clinical Bacterial Infection and Promoting Bone Formation. *ACS Appl. Mater. Interfaces* **2018**, *10*, 127–138. [CrossRef] [PubMed]
4. Ritz, U.; Gerke, R.; Götz, H.; Stein, S.; Rommens, P.M. A New Bone Substitute Developed from 3D-Prints of Polylactide (PLA) Loaded with Collagen I: An In Vitro Study. *Int. J. Mol. Sci.* **2017**, *18*, 2569. [CrossRef] [PubMed]
5. Zhang, C.; Zeng, B.; Zhu, K.; Zhang, L.; Hu, J. Limb salvage for malignant bone tumours of distal tibia with dual ipsilateral vascularized autogenous fibular graft in a trapezoid-shaped array with ankle arthrodesis and preserving subtalar joint. *Foot Ankle Surg.* **2019**, *25*, 278–285. [CrossRef]
6. Inzana, J.A.; Schwarz, E.M.; Kates, S.L.; Awad, H.A. Biomaterials approaches to treating implant-associated osteomyelitis. *Biomaterials* **2016**, *81*, 58–71. [CrossRef]
7. Zhang, Z.; Jia, B.; Yang, H.; Han, Y.; Wu, Q.; Dai, K.; Zheng, Y. Zn0.8Li0.1Sr—A biodegradable metal with high mechanical strength comparable to pure Ti for the treatment of osteoporotic bone fractures: In vitro and in vivo studies. *Biomaterials* **2021**, *275*, 120905. [CrossRef]
8. Avila, J.D.; Stenberg, K.; Bose, S.; Bandyopadhyay, A. Hydroxyapatite reinforced Ti6Al4V composites for load-bearing implants. *Acta Biomater.* **2021**, *123*, 379–392. [CrossRef]
9. Ke, D.; Vu, A.A.; Bandyopadhyay, A.; Bose, S. Compositionally graded doped hydroxyapatite coating on titanium using laser and plasma spray deposition for bone implants. *Acta Biomater.* **2018**, *84*, 414–423. [CrossRef]
10. Bunpetch, V.; Zhang, X.; Li, T.; Lin, J.; Maswikiti, E.P.; Wu, Y.; Cai, D.; Li, J.; Zhang, S.; Wu, C.; et al. Silicate-based bioceramic scaffolds for dual-lineage regeneration of osteochondral defect. *Biomaterials* **2019**, *192*, 323–333. [CrossRef]
11. Danışman, Ş.; Odabas, D.; Teber, M. The Effect of Coatings on the Wear Behavior of Ti6Al4V Alloy Used in Biomedical Applications. *IOP Conf.* **2018**, *295*, 012044. [CrossRef]

12. Li, M.; Xiong, P.; Yan, F.; Li, S.J.; Ren, C.H.; Yin, Z.C.; Li, A.; Li, H.F.; Ji, X.M.; Zheng, Y.F.; et al. An overview of graphene-based hydroxyapatite composites for orthopedic applications. *Bioact. Mater.* **2018**, *3*, 1–18. [CrossRef] [PubMed]
13. Mihalcea, E.; Vergara-Hernndez, H.J.; Jimenez, O.; Olmos, L.; Chavez, J.; Arteage, D. Design and characterization of Ti6Al4V/20CoCrMohighly porous Ti6Al4V biomedical bilayer processed by powder metallurgy. *Trans. Nonferrous Met. Soc. China* **2021**, *31*, 178–192. [CrossRef]
14. Ginebra, M.P.; Traykova, T.; Planell, J.A. Calcium phosphate cements: Competitive drug carriers for the musculoskeletal system. *Biomaterials* **2009**, *27*, 2171–2177. [CrossRef]
15. Poinern, G.E.; Brundavanam, R.K.; Mondinos, N.; Jiang, Z. Synthesis and characterisation of nanohydroxyapatite using an ultrasound assisted method. *Ultrason. Sonochem.* **2009**, *16*, 469–474. [CrossRef]
16. Ducheyne, P.; Radin, S.; King, L. The effect of calcium phosphate ceramic composition and structure on in vitro behavior. *I. Dissolution. J. Biomed. Mater. Res.* **2005**, *27*, 25–34. [CrossRef]
17. Liu, Q.B.; Zhu, W.; Zou, L.; Min, Z.; Dong, C. The effect of technological parameters of wide-band laser cladding on microstructure and sinterability of gradient bioceramics composite coating. *J. Biomed. Eng.* **2007**, *22*, 1193–1196.
18. Liu, Q.B.; Li, W.F.; Yang, B.C. Microstructure and Biocompatibility of Gradient Bioceramic Composite Coating Fabricated by Wide-Band Laser Cladding. *Key Eng. Mater.* **2009**, *342*, 685–688.
19. Liu, Q.B.; Wu, L.; Yang, B.C. Gradient Rare-Earths Bioceramic Composite Coating Fabricated by Wide-Band Laser Cladding and its Bioactivity. *Mater. Sci. Forum* **2009**, *610–613*, 1224–1226. [CrossRef]
20. Fu, Q.; Liu, Q.B.; Li, L.; Li, X.M.; Gu, H.Z.; Sheng, B. Effect of doping different Si source on Ca-P bioceramic coating fabricated by laser cladding. *J. Appl. Biomater. Fundam. Mater.* **2020**, *18*, 228080002091732. [CrossRef]
21. Fu, Q.; Liu, Q.B.; Li, L.; Li, X.M.; Gu, H.Z.; Sheng, B.; Yang, B.C. Study on microstructure, microhardness, bioactivity, and biocompatibility of La_2O_3-containing bioceramic coating doping SiO_2 fabricated by laser cladding. *J. Biomed. Mater. Res. Part B Appl. Biomater.* **2020**, *108*, 2099–2107. [CrossRef] [PubMed]
22. Zhang, S.; Liu, Q.B.; Li, L.; Bai, Y.; Yang, B.C. The controllable lanthanum ion release from Ca-P coating fabricated by laser cladding and its effect on osteoclast precursors. *Mater. Sci. Eng.* **2019**, *93*, 1027–1035. [CrossRef] [PubMed]
23. Vu, A.A.; Robertson, S.F.; Ke, D.; Bandyopadhyay, A.; Bose, S. Mechanical and biological properties of ZnO, SiO_2, and Ag_2O doped plasma sprayed hydroxyapatite coating for orthopaedic and dental applications. *Acta Biomater.* **2021**, *92*, 325–335. [CrossRef]
24. Geng, Z.; Ji, L.; Li, Z.; Wang, J.; He, H.; Cui, Z.; Yang, X.; Liu, C. Nano-needle strontium-substituted apatite coating enhances osteoporotic osseointegration through promoting osteogenesis and inhibiting osteoclastogenesis. *Bioact. Mater.* **2019**, *6*, 905–915. [CrossRef] [PubMed]
25. Qaid, T.H.; Ramesh, S.; Yusof, F.; Basirun, W.J.; Ching, Y.C.; Chandran, H.; Ramesh, S.; Krishnasamy, S. Micro-arc oxidation of bioceramic coatings containing eggshell-derived hydroxyapatite on titanium substrate. *Ceram. Int.* **2019**, *45*, 18371–18381. [CrossRef]
26. Gu, H.Z.; Fu, Q.; Sheng, B.; Cai, E.P.; Tang, G.; Liu, Q.B. Effect of pore-forming agent quantity on pore structure, phase composition, micro-hardness of gradient bioceramic coating under optimal laser process parameters. *Ceram. Int.* **2020**, *46*, 11275–11281. [CrossRef]
27. Hentrich, R.L.; Graves, G.A.; Stein, H.G.; Bajpai, P.K. An evaluation of inert and resorbale ceramics for future clinical orthopedic applications. *J. Biomed. Mater. Res.* **1971**, *5*, 25–51. [CrossRef]
28. Hench, L.L. The story of Bioglass. *J. Mater. Sci. Mater. Med.* **2016**, *17*, 967. [CrossRef]
29. Kang, M.H.; Jang, T.S.; Jung, H.D.; Kim, S.M.; Kim, S.M.; Koh, Y.H.; Song, J. Poly(ether imide)-silica hybrid coatings for tunable corrosion behavior and improved biocompatibility of magnesium implants. *Biomed. Mater.* **2016**, *11*, 035003. [CrossRef]
30. Jones, J.R. Review of bioactive glass: From Hench to hybrids. *Acta Biomater.* **2021**, *9*, 4457–4486. [CrossRef]
31. Li, X.; Lin, H.; Jiang, H.; Zhang, Y.; Liu, B.; Sun, Y.; Zhao, C. Preparation and properties of a new bio-based epoxy resin/diatomite composite. *Polym. Degrad. Stab.* **2021**, *187*, 109541. [CrossRef]
32. Liu, Q.B.; Zheng, M.; Zhu, W.; Li, H.; Dong, C. Microstructure and Properties on Gradient Bioceremics Composite Coating Produced by Wide- band Laser Cladding on Surface of Ti Alloy. *Appl. Laser.* **2004**, *24*, 350–354.
33. Sargeant, A.; Goswami, T. Hip implants: Paper V. Physiological effects. *Mater. Des.* **2018**, *27*, 287–307. [CrossRef]
34. Yoo, Y.S.; Kim, H.; Kim, D.Y. Effect of SiO_2 and TiO_2 addition on the exaggerated grain growth of $BaTiO_3$. *J. Eur. Ceram. Soc.* **2005**, *17*, 805–811. [CrossRef]
35. Maeno, S.; Niki, Y.; Matsumoto, H.; Morioka, H.; Yatabe, T.; Funayama, A.; Toyama, Y.; Taguchi, T.; Tanaka, J. The effect of calcium ion concentration on osteoblast viability, proliferation and differentiation in monolayer and 3D culture. *Biomater. Biomater. Guildf.* **2005**, *26*, 4847–4855. [CrossRef] [PubMed]
36. Kim, E.J.; Bu, S.Y.; Sung, M.K.; Kang, M.H.; Choi, M.K. Analysis of Antioxidant and Anti-inflammatory Activity of Silicon in Murine Macrophages. *Biol. Trace Elem. Res.* **2013**, *156*, 329–337. [CrossRef]
37. Kim, E.J.; Bu, S.Y.; Sung, M.K. Effects of Silicon on Osteoblast Activity and Bone Mineralization of MC_3T_3-E_1 Cells. *Biol. Trace Elem. Res.* **2003**, *152*, 105–112. [CrossRef]
38. Porter, A.E.; Patel, N.; Skepper, J.N.; Best, S.M.; Bonfield, W. Comparison of in vivo dissolution processes in hydroxyapatite and silicon-substituted hydroxyapatite bioceramics. *Biomaterials* **2003**, *24*, 4609–4620. [CrossRef]
39. Lin, K.; Liu, Y.; Huang, H.; Chen, L.; Wang, Z.; Chang, J. Degradation and silicon excretion of the calcium silicate bioactive ceramics during bone regeneration using rabbit femur defect model. *J. Mater. Sci. Mater. Med.* **2015**, *26*, 197. [CrossRef]

40. Wu, C.; Fan, W.; Zhou, Y.; Lou, Y.X.; Gelinsky, M.; Chang, J.; Xiao, Y. 3D-printing of highly uniform $CaSiO_3$ ceramic scaffolds: Preparation, characterization and in vivo osteogenesis. *J. Mater. Chem.* **2012**, *22*, 12288–12295. [CrossRef]
41. Matesanz, M.C.; Linares, J.; Lilue, I.; Salcedo, S.S.; Feito, J.M.; Arcos, D.; Regi, V.M.; Portoles, T.M. Nanocrystalline silicon substituted hydroxyapatite effects on osteoclast differentiation and resorptive activity. *J. Mater. Chem.* **2014**, *19*, 2910–2919. [CrossRef] [PubMed]
42. Zhou, P.; Xia, D.; Ni, Z.; Ou, T.; Wang, Y.; Zhang, H.; Mao, L.; Lin, K.; Xu, S.; Liu, J. Calcium silicate bioactive ceramics induce osteogenesis through oncostatin M. *Bioact. Mater.* **2021**, *6*, 810–822. [CrossRef] [PubMed]
43. Kokubo, T.; Kim, H.M.; Kawashita, M.; Nakamura, T. Bioactive metals: Preparation and properties. *J. Mater. Sci. Mater. Med.* **2004**, *15*, 99–107. [CrossRef] [PubMed]
44. Chen, W.; Yang, X.; Lin, K.; Lu, J.; Chang, J.; Sun, J. The enhancement of bone regeneration by a combination of osteoconductivity and osteostimulation using β-$CaSiO_3$/β-$Ca_3(PO_4)_2$ composite bioceramics. *Acta Biomater.* **2012**, *8*, 350–360.
45. Lu, W.; Duan, W.; Guo, Y.; Ning, C. Mechanical Properties and In Vitro Bioactivity of $Ca_5(PO_4)_2SiO_4$ Bioceramic. *J. Biomater. Appl.* **2012**, *26*, 637–650. [CrossRef]
46. Ni, S.; Lin, K.; Chang, J.; Chou, L. β-$CaSiO_3$/β-$Ca_3(PO_4)_2$ composite materials for hard tissue repair: In vitro studies. *J. Biomed. Mater. Res. Part A* **2008**, *85A*, 72–82. [CrossRef]
47. He, F.; Ye, T. Improvements in phase stability and densification of β-tricalcium phosphate bioceramics by strontium-containing phosphate-based glass additive. *Ceram. Int.* **2018**, *44*, 11622–11627. [CrossRef]
48. Champion, E. Sintering of calcium phosphate bioceramics. *Acta Biomater.* **2013**, *9*, 5855–5875. [CrossRef]